

PROMPT GEV-TeV EMISSION OF GAMMA-RAY BURSTS DUE TO HIGH-ENERGY PROTONS, MUONS AND ELECTRON-POSITRON PAIRS

KATSUAKI ASANO AND SUSUMU INOUE

Division of Theoretical Astronomy, National Astronomical Observatory of Japan, 2-21-1 Osawa, Mitaka, Tokyo 181-8588, Japan
Draft version August 23, 2021

ABSTRACT

In the framework of the internal shock scenario, we model the broadband prompt emission of gamma-ray bursts (GRBs) with emphasis on the GeV-TeV bands, utilizing Monte Carlo simulations that include various processes associated with electrons and protons accelerated to high energies. While inverse Compton emission from primary electrons is often dominant, different proton-induced mechanisms can also give rise to distinct high-energy components, such as synchrotron emission from protons, muons or secondary electrons/positrons injected via photomeson interactions. In some cases, they give rise to double spectral breaks that can serve as unique signatures of ultra-high-energy protons. We discuss the conditions favorable for such emission, and how they are related to the production of ultra-high-energy cosmic rays and neutrinos in internal shocks. Ongoing and upcoming observations by *GLAST*, atmospheric Cerenkov telescopes and other facilities will test these expectations and provide important information on the physical conditions in GRB outflows.

Subject headings: gamma rays: bursts — gamma rays: theory — radiation mechanisms: nonthermal — cosmic rays — neutrinos

1. INTRODUCTION

The prompt emission of gamma-ray bursts (GRBs) is characterized by rapid temporal variability and nonthermal spectra extending to high energies, implying an origin in ultrarelativistic outflows with bulk Lorentz factors $\Gamma \gtrsim 100$ (see, e.g., reviews by Piran 2005; Mészáros 2006). In the widely discussed internal shock scenario, collisions among inhomogeneities within the flow lead to formation of shocks that convert bulk kinetic energy into Fermi-accelerated, power-law distributions of relativistic electrons, which then emit synchrotron photons to be observed as the MeV-range gamma-rays (Rees & Mészáros 1994). However, a number of challenges for the internal shock model have been pointed out concerning the radiative efficiency, low energy spectral slope, various kinds of luminosity correlations, etc., and very different alternative models have been proposed (Piran 2005; Mészáros 2006; Fox & Mészáros 2006, and references therein). In order to unravel the true nature of the prompt emission as well as to constrain important physical quantities such as Γ and magnetic fields in the outflow, more broadband observations including the GeV-TeV bands are warranted.

The physical conditions inferred for internal shocks indicate that protons may be Fermi-accelerated to energies $\sim 10^{20}$ eV, making GRBs potential sources of the observed ultra-high-energy cosmic rays (UHECRs; Waxman 1995; Vietri 1995). To test the GRB origin of UHECRs and distinguish it from other possibilities (Torres & Anchordoqui 2004; Inoue 2007), it is essential to search for characteristic, UHE proton-induced signatures of secondary neutral radiation that can be observed in coincidence with GRBs. Besides production of high-energy neutrinos (Waxman & Bahcall 1997; Mészáros & Razzaque 2006, and references therein), efficient proton acceleration may

induce distinctive emission components in the GeV-TeV bands (Zhang & Mészáros 2004; Piran 2005; Mészáros 2006; Dermer & Atoyan 2006, and references therein).

So far, observational information on GRB GeV-TeV emission has been quite limited. The *EGRET* instrument onboard *CGRO* was able to detect GeV emission from just a handful of the brightest bursts (Hurley et al. 1994; Dingus 2001; González et al. 2003). No strong evidence of emission in the TeV region has been found to date (e.g. Connaughton et al. 1997; Atkins et al. 2005; Albert et al. 2007; Horan et al. 2007), but this could be largely due to the generally high redshifts of GRBs and the consequent attenuation by pair production with extragalactic background radiation (e.g. Mannheim et al. 1996).

However, significant advances are expected soon with the launch of *GLAST*¹, with greatly improved sensitivity and wider field of view at GeV energies. TeV emission from bursts at sufficiently low redshift may eventually be discovered through ongoing observations with current Cerenkov telescopes such as H.E.S.S.², VERITAS³, CANGAROO III⁴, and especially MAGIC⁵ with its 50 GeV threshold and fast slewing capabilities, as well as all-sky detectors such as MILAGRO⁶.

In anticipation of the observational progress, this paper discusses detailed theoretical modeling of GRB prompt emission in the context of the internal shock scenario, focusing on the GeV-TeV bands. Monte Carlo techniques are employed to account for cascade processes involving photon-photon ($\gamma\gamma$) pair production and Klein-Nishina regime Compton scattering, as well as proton-induced processes such as photomeson interactions and

¹ <http://glast.gsfc.nasa.gov/>

² <http://www.mpi-hd.mpg.de/hfm/HESS/HESS.html>

³ <http://veritas.sao.arizona.edu/>

⁴ <http://icrhp9.icrr.u-tokyo.ac.jp/>

⁵ <http://magic.mppmu.mpg.de/>

⁶ <http://www.lanl.gov/milagro/>

secondary pion, muon, electron and positron injection. Although various aspects of high energy emission from internal shocks have been covered in previous studies (e.g. Papathanassiou & Mészáros 1996; Pilla & Loeb 1998; Guetta & Granot 2003; Pe'er & Waxman 2004b; Razzaque et al. 2004; Baring 2006), few have discussed hadronic cascade processes in such detail.

In §2, our model assumptions, methods and choice of parameters are explained. §3 summarizes some general aspects of the high-energy cutoff and inverse Compton emission. The effects induced by high-energy protons are highlighted in §4, and the relation between GeV-TeV emission and UHECR and neutrino production is discussed in §5. We briefly touch on the observational implications in §6, and conclude in §7.

2. MODEL DESCRIPTION

2.1. Model Assumptions and Numerical Methods

In the internal shock picture, each pulse observed in the MeV light curve of GRBs is interpreted as emission from shocks formed in collisions between material travelling at different velocities (Kobayashi et al. 1997; Daigne & Mochkovitch 1998). Here we do not deal with the dynamics of the shocks and instead concentrate on the emission properties. The emitting region for a pulse is considered to be a homogeneous shell expanding with Γ at radii R from the central engine. We adopt $l = R/\Gamma$ for the comoving width of the shell, so that the pulse timescale in the observer frame is $\Delta t = R/\Gamma^2 c$ (Sari & Piran 1997), (see however Asano & Iwamoto 2002). Note that our spherically symmetric formulation is equally valid for a collimated outflow so long as the collimation angle $\gg 1/\Gamma$.

Detailed modeling of the GRB spectra including the rapid, irregular time variability would entail considerable complexity. In this work, we choose not to consider the time variability in earnest and assume steady state conditions, at least during the pulse timescale Δt . For bursts composed of multiple pulses, we also assume for simplicity that all pulses within a burst are similar, i.e. they are emitted from N shells with identical physical conditions. Our results are therefore to be interpreted as the time-averaged spectra for each burst.

We employ the Monte Carlo numerical code of Asano (2005) and Asano & Nagataki (2006), newly supplemented with $\gamma\gamma$ pair production and synchrotron self-absorption. All photons and particles (electrons, positrons, protons, pions, muons) are distributed isotropically in the shell frame and treated in the one-zone approximation. Being mutually affected through processes such as photomeson interactions and inverse Compton (IC) scattering, the energy distributions of photons and particles are simulated iteratively until they converge to a self-consistent steady state, which is assumed to be realized within the pulse timescale.

The energy density of accelerated electrons in the shell U_e is a parameter that can be directly related to observables (§2.2). The magnetic field strength B is parameterized by f_B so that its energy density $U_B \equiv B^2/8\pi = f_B U_e$. Electrons are injected with a power-law energy distribution $N(\gamma_e) \propto \gamma_e^{-p_e}$ in the range $\gamma_{e,\min} \leq \gamma_e \leq \gamma_{e,\max}$, where γ_e is the electron Lorentz factor in the shell frame. The minimum Lorentz factor

$\gamma_{e,\min}$ is often evaluated in the literature by giving U_e together with the total number density n_e of electrons in the shell, which can be related to the dissipated kinetic energy (e.g. Kobayashi et al. 1997). Instead of considering n_e , here we take $\gamma_{e,\min}$ to be an additional parameter, the value of which can be inferred from the observed spectral peak energy (§2.2). The maximum Lorentz factor $\gamma_{e,\max}$ is where synchrotron and IC losses limit Fermi acceleration. However, its value is not very crucial here, since our choice of p_e below (§2.2) implies that other factors are more important in shaping the high energy spectra.

Accelerated protons with energy density U_p are also injected with a power-law energy distribution $\propto \gamma_p^{-p_p}$ ($\gamma_{p,\min} \leq \gamma_p \leq \gamma_{p,\max}$) in the shell frame. The maximum proton Lorentz factor $\gamma_{p,\max}$ is determined by equating $t_{\text{acc}} = \gamma_p m_p c^2 / e B c$, the Fermi acceleration timescale in relativistic shocks (e.g. Waxman 1995), to $\min[t_{\text{exp}}, t_{\text{loss}}]$, where $t_{\text{exp}} = R/\Gamma c$ is the comoving expansion timescale and t_{loss} is the energy loss timescale due to synchrotron, IC, and photomeson cooling, as described in Asano (2005). The minimum proton Lorentz factor $\gamma_{p,\min}$ is expected to be of order unity in internal shocks with typically mildly relativistic velocities; here we take $\gamma_{p,\min} = 10$, although the exact value is irrelevant for the resulting spectra.

As in Asano & Nagataki (2006), we utilize experimental results for the cross sections of the reactions $p\gamma \rightarrow n\pi^+$, $p\pi^0$, $n\pi^+\pi^0$, and $p\pi^+\pi^-$ for $\varepsilon' \leq 2$ GeV, where ε' is the photon energy in the proton rest frame (Schadmand 2003). The process $p\gamma \rightarrow p\pi^0\pi^0$ is neglected due to its small cross section. For pion production by $n\gamma$ reactions, we adopt the same cross sections as the respective $p\gamma$ channels. The inelasticity is approximated by $K = [1 - (m_p^2 - m^2)/s]/2$, where s is the center-of-momentum energy squared for the $p\gamma$ or $n\gamma$ system, $m = m_\pi$ and $m = 2m_\pi$ for single and double pion production, respectively, and m_π is the pion mass. Pion production via pp collisions is not considered here since target photons always greatly outnumber protons.

We account for the decay of pions and muons and associated electron/positron injection as well as synchrotron and IC emission from all charged particles with the methods of Asano (2005). The full Klein-Nishina cross section (e.g. Blumenthal & Gould 1970) is employed for IC scattering. For synchrotron radiation from very high-energy electrons/positrons, quantum effects can become important. When the classical value for the synchrotron photon energy $\varepsilon_{\text{syn}} = \gamma_e^2 \hbar e B / m_e c$ is larger than 10% of the particle energy $\gamma_e m_e c^2$, we use approximate emissivity formulae following Erber (1966). The details of this treatment do not affect the results significantly, as such synchrotron photons promptly create further pairs and the initial information is lost in the cascade process. For the same reason, we also do not distinguish between the cascade contributions from pions and muons.

Newly implemented here into the Monte Carlo code with the appropriate cross sections are $\gamma\gamma$ pair production and synchrotron self-absorption by electrons/positrons. The cross section for $\gamma\gamma$ pair production is $\sigma_{\pm} = \sigma_T g(y)$, where σ_T is the Thomson cross section,

$$g(y) \equiv \frac{3}{16} (1-y^2) \left[(3-y^4) \ln \frac{1+y}{1-y} - 2y(2-y^2) \right], \quad (1)$$

y is given by $y^2 = 1 - (2m_e^2 c^4)/[\varepsilon_1 \varepsilon_2 (1 - \cos \theta)]$, ε_1 and ε_2 are the energies of the two photons and θ is their incident angle (Berestetskii et al. 1982). For synchrotron absorption of an isotropic photon field by electrons/positrons, the differential cross sections for true absorption and stimulated emission are respectively

$$\frac{d\sigma_a}{d\Omega}(\gamma_e, \varepsilon_0) = \frac{c^2 h^3 \gamma_e' u_e'}{8\pi \varepsilon_0^3 \gamma_e u_e} P(\gamma_e', \varepsilon_0), \quad (2)$$

$$\frac{d\sigma_s}{d\Omega}(\gamma_e, \varepsilon_0) = \frac{c^2 h^3}{8\pi \varepsilon_0^3} P(\gamma_e, \varepsilon_0), \quad (3)$$

where ε_0 is the photon energy, $\gamma_e' = \gamma_e + \varepsilon_0/m_e c^2$, $u_e = (\gamma_e^2 - 1)^{1/2}$, $u_e' = (\gamma_e'^2 - 1)^{1/2}$, and $P(\gamma_e, \varepsilon_0)$ is the synchrotron power per unit photon energy (Ghisellini & Svensson 1991). An accurate treatment of synchrotron self-absorption is necessary to determine the correct photon spectrum at very low energies, which in turn is essential for properly evaluating the photomeson interaction rate for UHE protons.

We do not include pair annihilation, which can lead to a prominent spectral component for sufficiently high compactness parameters, but only in a narrow energy range around $\Gamma m_e c^2$ (Pe'er & Waxman 2004b).

2.2. Constraints on Parameters

The full set of our model parameters consists of Γ , R , N , U_e , f_B , $\gamma_{e,\min}$, p_e , U_p and p_p . For Γ and R , we consider the ranges $\Gamma = 30$ -1000 and $R = 10^{13}$ - 10^{16} cm, as generally discussed for internal shock models (e.g. Mészáros & Rees 2000). We assume a range of $f_B = 0.1$ -30 for the magnetic field (see below). In order to keep the scope of the current study tractable, some combinations of the remaining parameters are constrained so as to reproduce typically observed properties of the MeV, primary synchrotron component.

For given values of B and Γ , $\gamma_{e,\min}$ is chosen so that the corresponding synchrotron photon energy in the observer frame $\varepsilon_{\text{pk}} = \Gamma \gamma_{e,\min}^2 \hbar e / m_e c$ is always 300 keV (for GRB redshift $z = 0.1$, see below). The electron injection index is fixed to $p_e = 3$, implying that in the fast-cooling conditions of internal shocks, the photon index immediately above ε_{pk} is $\beta = -(p_e + 2)/2 = -2.5$, the mean value measured by BATSE (Preece et al. 2000).

During the pulse timescale Δt , the fast-cooling electrons reach steady state where $U_e \simeq U_{\gamma,e}$, the energy density of photons emitted by electrons in the shell rest frame. The isotropic-equivalent energy of photons from a single pulse is thus $E_{\text{sh},e} = 4\pi \Gamma^2 U_{\gamma,e} R^2 c \Delta t \simeq 4\pi R^3 U_e$. In all cases studied below, the emitted luminosity is dominated by MeV synchrotron photons, so for given R , U_e can be related to the observable MeV pulse energy E_{sh} . Hereafter U_e is replaced by E_{sh} as a parameter in the range 10^{50} - 10^{52} erg. Under our assumption of N identical pulses constituting a burst (§2.1), the time-integrated, isotropic-equivalent photon energy for a burst is $E_{\text{tot}} = N E_{\text{sh}}$, which we fix to a typical value of 10^{53} erg.

Although the proton component cannot be strongly constrained from existing observations, we assume $U_p = U_e$ and $p_p = 2$, which are necessary conditions for GRBs to be energetically viable as UHECR sources (Waxman 1995; Vietri 1995). (However, recent observations may

suggest larger values of U_p , §5.) The proton spectral index p_p is expected to be similar to p_e at low energies where the particle gyroradii overlap, but this may not necessarily be the case at ultra-high-energies that are important for photomeson interactions. In particular, if the nonlinear back-reaction of CR pressure on the shock structure is significant, a concave spectral shape may result that is much harder at high energies compared to low energies (Malkov & Drury 2001), even though the details are uncertain for relativistic shocks (Baring & Kirk 1991).

After specifying the observables ε_{pk} , β and E_{tot} to typical values and making plausible assumptions for the protons, the remaining variable parameters are Γ , R , f_B and E_{sh} . Utilizing the observable pulse timescale $\Delta t = R/\Gamma^2 c$ instead of R , we choose to characterize our results with the set of Δt , E_{sh} , Γ and f_B . Note that a relation can also be made to the pulse luminosity $L = E_{\text{sh}}/\Delta t$.

All spectra below are shown in terms of the observed fluence versus photon energy, assuming a GRB redshift of $z = 0.1$. We do not include spectral attenuation by pair production with the extragalactic infrared background, which may be justified at $z \lesssim 0.1$ and $\varepsilon \lesssim 3$ TeV (Aharonian et al. 2006), but should be more important for higher redshifts and photon energies. The potential effects of intergalactic cascade emission (e.g. Plaga 1995; Razzaque et al. 2004; Wang et al. 2004; Casanova et al. 2007; Murase et al. 2007) are also neglected.

We caution that actual GRBs are observed with considerable dispersions in ε_{pk} , β and E_{tot} , notwithstanding a good correlation between ε_{pk} and E_{tot} (Amati 2006). Pulses within each burst can also exhibit a variety of properties. Such aspects need to be accounted in future, more comprehensive studies.

Note that cases of $f_B = U_B/U_e \gg 1$ can be compatible with internal shocks in a kinetic energy-dominated outflow, as long as the fraction of protons and electrons injected into the acceleration process is sufficiently small, and most of the outflow energy remains in the form of cold or thermal protons. Indeed, the typical radiative efficiency expected from electrons accelerated in internal shocks is only a few percent (e.g. Daigne & Mochkovitch 1998) (see however Zhang et al. 2007), so that f_B as large as 30 may still be consistent with this picture. Even in magnetically-dominated flows, shocks can occur under certain conditions (Zhang & Kobayashi 2005).

3. HIGH-ENERGY CUTOFF AND INVERSE COMPTON EMISSION

Before proton-induced effects are addressed in detail in §4, we discuss some generic aspects of the high-energy spectral cutoff that are independent of the emission mechanism, together with the properties of GeV-TeV spectra in the typical case where inverse Compton emission from electrons dominate.

3.1. High-Energy Cutoff

In Fig. 1, we show exemplary spectra for the case of $\Delta t = 0.1$ s, $E_{\text{sh}} = 10^{51}$ erg, and different values of Γ and f_B . Above the synchrotron peak at $\varepsilon_{\text{pk}} = 300$ keV, there are varying levels of a second high-energy component, here all due to inverse Compton emission. Clear spec-

tral cut-offs can be seen at the highest energies, above where pair production with low energy photons within the emission region strongly attenuates the spectrum.

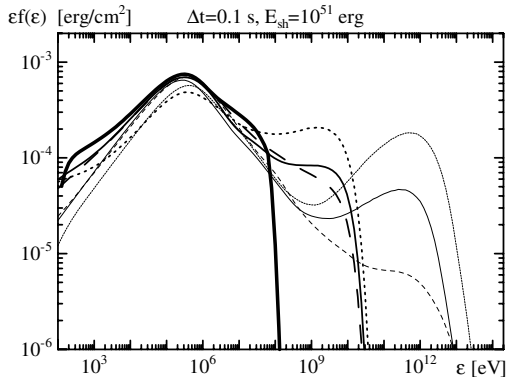


FIG. 1.— Spectra for $\Delta t = 0.1$ s, $E_{\text{sh}} = 10^{51}$ erg and varying Γ and f_B . The thickest curve is for $\Gamma = 100$ and $f_B = 1.0$. The medium-thick and thin curves are for $\Gamma = 300$ and 1000 , respectively, while dotted, solid and dashed each correspond to $f_B = 0.1$, 1, and 30.

The high-energy cutoff energy ε_{cut} should provide an effective probe of the bulk Lorentz factor Γ , as has been discussed previously (e.g. Baring & Harding 1997; Lithwick & Sari 2001). For the case of a pure power-law spectrum, Asano & Takahara (2003) have obtained an analytical expression, $\varepsilon_{\text{cut}} \propto \Gamma^{14/3} E_{\text{sh}}^{-2/3} \Delta t^{4/3}$ for $p_e = 3$ (or $\varepsilon_{\text{cut}} \propto \Gamma^{26/5} E_{\text{sh}}^{-4/5} \Delta t^{8/5}$ for $p_e = 5/2$). Our Monte Carlo simulation results reveal values of ε_{cut} that are too scattered to be fit well by one simple, analogous formula. Nevertheless, it can be approximated roughly by

$$\varepsilon_{\text{cut}} \simeq 10^9 \left(\frac{\Gamma}{100} \right)^4 \left(\frac{E_{\text{sh}}}{10^{51} \text{erg}} \right)^{-0.5} \left(\frac{\Delta t}{1 \text{s}} \right)^{1.3} \text{eV}, \quad (4)$$

with a typically strong Γ -dependence. Thus, together with the observables Δt and E_{sh} (or L), measurements of ε_{cut} should provide tight constraints on Γ . These inferences are mostly independent of the emission process that shape the GeV-TeV spectra, whether IC or not.

3.2. Inverse Compton Emission

Detecting the IC component should be crucial for probing the magnetic field strength, especially for larger values of Γ . For $\Gamma = 300$ -1000 in Fig. 1, the strong dependence of the IC fluence on f_B is apparent. For lower f_B and consequently higher IC fluence, the synchrotron fluence is somewhat suppressed due to the greater importance of IC cooling. In contrast, for $\Gamma = 100$, the spectra for different $f_B = 0.1$ -30 are almost indistinguishable, as ε_{cut} occurs at too low energies for the IC component to be clearly discerned. Here the dominant high-energy component is simply the extension of the primary synchrotron emission up to $\varepsilon_{\text{cut}} \sim 0.1$ GeV.

Fig. 2 displays more details of the spectra for a case where IC emission makes a distinct second peak at $\varepsilon \sim 10$ GeV. The IC to synchrotron peak fluence ratio is less than the simple Thomson limit expectation

$\propto U_e/U_B = f_B^{-1}$ because of the Klein-Nishina effect and $\gamma\gamma$ absorption. Note that “electrons” here include both primary electrons, i.e. those directly accelerated at the shocks, as well as additional pairs that are injected by $\gamma\gamma$ interactions at higher energies.

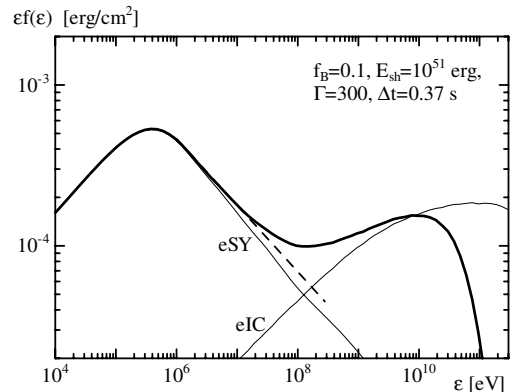


FIG. 2.— Spectrum for a case with inverse Compton peak (thick solid), for $\Delta t = 0.37$ s, $E_{\text{sh}} = 10^{51}$ erg, $\Gamma = 300$ and $f_B = 0.1$. Thin curves denote separately electron synchrotron (labeled eSY) and inverse Compton (labeled eIC) components, without $\gamma\gamma$ absorption effects. The dashed line is a power-law extrapolation of the MeV-range spectrum.

These results on IC emission from internal shocks are broadly consistent with previous, more approximate studies (e.g. Papathanassiou & Mészáros 1996; Pilla & Loeb 1998; Guetta & Granot 2003). In §A, we show some quantitative relations for the spectral peak energies and fluence ratios in our model, which might offer a useful consistency check of the internal shock scenario, at least within the parameter space studied here.

4. PROTON-INDUCED HIGH-ENERGY EMISSION

For the range of parameters covered in this study (§2.2), IC emission often turns out to be the dominant high-energy emission mechanism (see Figs. 7, 8). Nevertheless, we find that within plausible parameter regimes, distinctive spectral features can emerge at GeV-TeV energies due to characteristic processes induced by UHE protons.

One potential radiative signature of UHE protons in GRBs is their synchrotron emission, first proposed by Vietri (1997). Fig. 3 is a case with relatively high magnetic fields ($f_B = 30$), in which proton synchrotron emission makes a marked contribution to the spectrum at $\varepsilon \sim 1$ -100 GeV. Although the spectral bump here is not as prominent as some examples of IC peaks (§3.2), it forms a clear excess above a simple extrapolation of the MeV-band spectrum that may be detectable by GLAST, MAGIC and other facilities.

Another example with high magnetic fields ($f_B = 30$) is shown in Fig. 4. Here, a notable hardening of the spectrum can be seen at $\varepsilon \sim 0.01$ -1 GeV, caused by synchrotron emission from secondary pairs injected by photomeson interactions. Since primary electrons alone cannot give rise to such distinct features, this is a unique

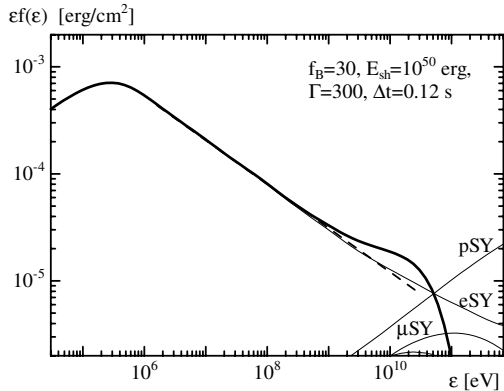


FIG. 3.— Spectrum for a case with proton synchrotron bump (thick solid), for $\Delta t = 0.12$ s, $E_{\text{sh}} = 10^{50}$ erg, $\Gamma = 300$ and $f_B = 30$. Thin curves denote separately electron synchrotron (eSY), proton synchrotron (pSY) and muon synchrotron (μ SY) components, without $\gamma\gamma$ absorption effects. The dashed line is a power-law extrapolation of the MeV-range spectrum.

effect triggered by UHE protons, which has not been discussed before for GRB prompt emission. Note that in order to correctly evaluate the density of low-energy target photons for the $p\gamma$ process, it is imperative to include self-absorption effects in the electron synchrotron spectrum (§2.1).

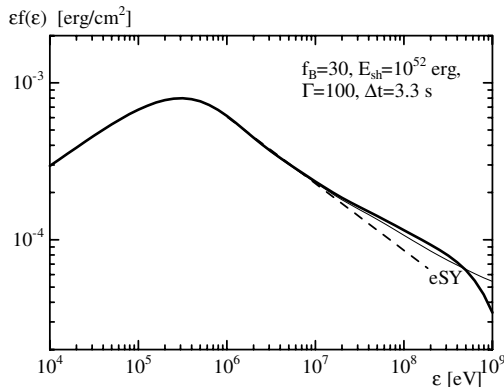


FIG. 4.— Spectrum for a case with secondary pair synchrotron bump (thick solid), for $\Delta t = 3.3$ s, $E_{\text{sh}} = 10^{52}$ erg, $\Gamma = 100$ and $f_B = 30$. Thin curve denotes the synchrotron component (eSY) without $\gamma\gamma$ absorption effects. The dashed line is a power-law extrapolation of the MeV-range spectrum.

Although such features should serve as valuable indicators of UHE protons in GRBs, it may not be easy from spectral measurements alone to distinguish them from some cases of IC emission. However, under certain conditions, more than one emission mechanism can become simultaneously important and lead to double spectral breaks, which can only occur in the presence of accelerated protons. Fig. 5 is an example where the spectrum hardens above a first break at ~ 0.01 GeV from secondary pair synchrotron emission, and then hardens

further above a second break at ~ 0.1 GeV from IC emission. Spectra with such double breaks may offer crucial observational evidence for UHE proton acceleration.

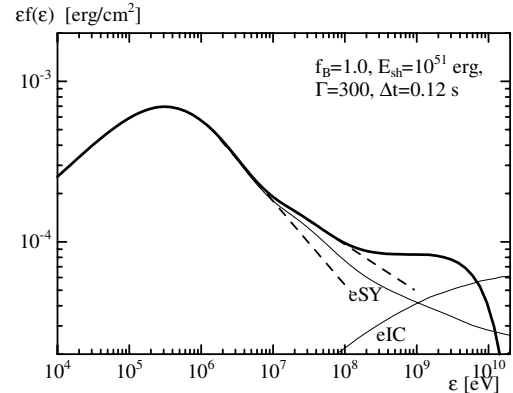


FIG. 5.— Spectrum for a case with double breaks due to secondary pair synchrotron and IC emission (thick solid), for $\Delta t = 0.12$ s, $E_{\text{sh}} = 10^{51}$ erg, $\Gamma = 300$ and $f_B = 1$. Thin curves denote separately electron synchrotron (eSY) and IC (eIC) components, without $\gamma\gamma$ absorption effects. The dashed lines are power-law extrapolations of the spectra in the ranges 1-10 MeV and 10-100 MeV.

Yet a third proton-induced process that can be significant is synchrotron emission from muons injected by $p\gamma$ interactions, first discussed by Asano & Takahara (2003). In Fig. 6, again for high magnetic fields ($f_B = 30$), a muon synchrotron spectral bump is eminent at $\epsilon \sim 10$ -100 GeV. Additionally visible in this case are secondary pair synchrotron emission at $\epsilon \sim 0.1$ -1 GeV, proton synchrotron emission at $\epsilon \sim 100$ GeV, and even a minor contribution from pion synchrotron emission at $\epsilon \gtrsim 100$ GeV, illustrating the spectral variety generated by UHE protons. While not shown here, there are other instances where muon synchrotron is the sole high-energy component (see §B).

It is important to clarify in which physical regimes of GRB internal shocks these proton-related emission components become clearly visible. Here we do not attempt to explore the full parameter space, but choose to map out certain ranges of Γ and f_B while focusing on the following two sets of Δt and E_{sh} : (1) “spiky pulse” case of $\Delta t = 0.1$ s and $E_{\text{sh}} = 10^{51}$ erg, (similar to Figs. 3, 4 and 5), and (2) “broad pulse” case of $\Delta t = 10^{0.5}$ s and $E_{\text{sh}} = 10^{52}$ erg. Whenever IC, proton synchrotron or secondary pair synchrotron emission create distinct spectral features over the extrapolated MeV-range spectra, we correspondingly indicate “IC”, “PS” or “SS” in the f_B - Γ plane of Figs. 7 and 8. When two components occur simultaneously, they are indicated together with a “+” sign, while black dots signify that no separate high-energy component is discernible. (Muon synchrotron emission does not become significant in these two cases, but can be evident for other Δt and E_{sh} as in Fig. 6.)

Generally speaking, we see that GeV-TeV emission requires sufficiently large Γ regardless of the emission

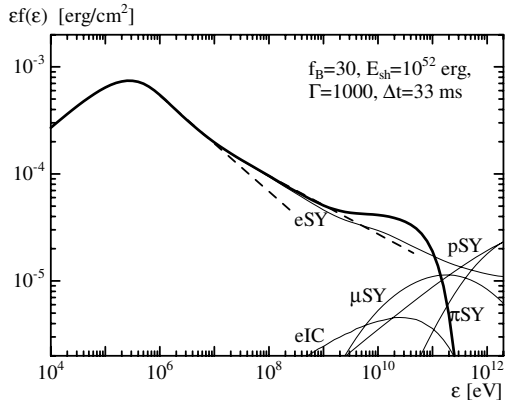


FIG. 6.— Spectrum for a case with muon synchrotron bump (thick solid), for $\Delta t = 33$ ms, $E_{\text{sh}} = 10^{52}$ erg, $\Gamma = 1000$ and $f_B = 30$. Thin curves denote separately electron synchrotron (eSY), IC (eIC), proton synchrotron (pSY), muon synchrotron (μ SY), and pion synchrotron (π SY) components, without $\gamma\gamma$ absorption effects. The dashed lines are power-law extrapolations of the spectra in the ranges 1-10 MeV and 10-100 MeV.

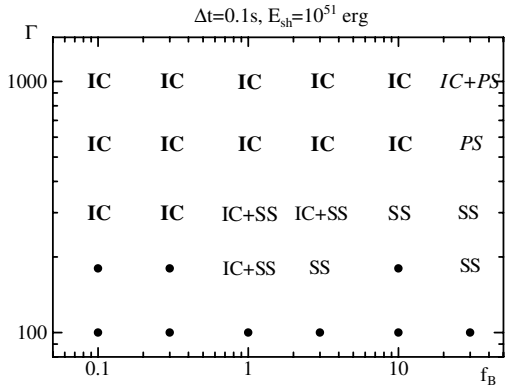


FIG. 7.— Summary of visible high-energy spectral components in the f_B - Γ plane, denoted by IC (inverse Compton), PS (proton synchrotron) and SS (secondary pair synchrotron), for $\Delta t = 0.1$ s and $E_{\text{sh}} = 10^{51}$ erg (spiky pulse case). Black dots imply no distinct high-energy feature.

mechanism to avoid $\gamma\gamma$ absorption (§3.1), and that larger f_B is more conducive to proton-induced components. We also see that cases of multiple components can be fairly common. A more quantitative summary of the model spectra in the current study can be found in §B, which may provide a guide to searches for proton-induced signals in future observations.

While proton-induced emission can become clearly observable, in all the cases studied here, it does not lead to conspicuously separate spectral peaks as for the IC emission. On the other hand, such situations may be possible outside of the parameter restrictions we set in §2.2. For example, some recent observations may point to $U_p > U_e$ if GRBs are the origin of UHECRs (§5). All proton-related components will then be duly increased,

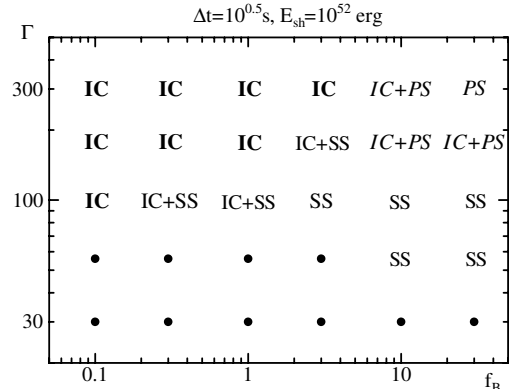


FIG. 8.— Same as Fig.7, but for $\Delta t = 10^{0.5}$ s and $E_{\text{sh}} = 10^{52}$ erg (broad-pulse case).

as they simply scale in proportion to U_p .

Although not explicitly addressed in this work, we mention that time variability should also be a crucial diagnostic of emission mechanisms, as each process has its characteristic timescale and dependence on photon energy. This will be an important subject for future studies.

5. RELATION TO ULTRA-HIGH-ENERGY COSMIC RAY AND NEUTRINO PRODUCTION

We now discuss how the above results on GeV-TeV emission are related to the processes of UHECR and neutrino production in GRB internal shocks. Since the internal shock model entails a wide range of physical conditions by design, the circumstances most favorable for each process are not necessarily the same. We concentrate below on some representative cases without investigating the full model parameter space.

The acceleration of protons to ultra-high energies is a necessary but not sufficient condition for GRB internal shocks to be significant contributors of UHECRs, since the particles must also escape efficiently without suffering significant energy losses. Although a detailed description of UHECR escape is beyond the scope of this paper, following Asano (2005), we can impose a relevant constraint that the particles in question, say, protons with energy $\varepsilon_p \geq 10^{19}$ eV, do not lose more than half of their energy radiatively in a comoving expansion timescale after their injection in the shell (roughly $t_{\text{loss}} \gtrsim t_{\text{exp}}$). Strictly speaking, this is a minimum requirement, but if it is satisfied, we may expect that the higher energy particles can eventually escape as the shell expands and both the photon density and magnetic field drop rapidly (note $B \propto R^{-3/2}$). We can then infer a lower bound on the shell radius R , or equivalently on Γ for given Δt and E_{sh} . From our numerical results, this criterion for efficient UHECR production is approximately $R \gtrsim 10^{14} (E_{\text{sh}}/10^{50} \text{ erg})^{0.5} (\Gamma/300)^{-1}$ cm or $\Gamma \gtrsim 300 (\Delta t/0.1 \text{ s})^{-0.3} (E_{\text{sh}}/10^{51} \text{ erg})^{0.2}$. The dependence on the magnetic field parameter f_B is weak as the losses are mostly due to photomeson interactions rather than synchrotron radiation (although the latter becomes more important for higher energies $\varepsilon_p \gtrsim 10^{20}$ eV). Note

that effective particle escape via neutron conversion is included in this criterion and only occurs in a narrow parameter range near the lower limit values.

Turning to gamma-ray emission, we saw that distinct GeV-TeV components mandate high values of Γ from $\gamma\gamma$ optical depth constraints, irrespective of the emission mechanism (§3.1). In fact, the above bound on Γ for UHECR production roughly matches the bound from gamma-rays, at least for the two exemplary cases of Δt and E_{sh} in §4 (regions outside the black dots in the f_B - Γ plane of Figs. 7 and 8). Therefore, the appearance of even the IC emission may possibly indicate that the physical conditions are also appropriate for efficient UHECR acceleration and escape. Of course, the emergence of proton-induced emission (only for high f_B) will be most valuable as it can directly probe important quantities such as U_p/U_e and $\gamma_{p,\text{max}}$.

Detection of high-energy neutrinos is often emphasized as a definitive observational test of the GRB origin of UHECRs (Halzen & Hooper 2002). However, the situation most advantageous for neutrino production is that UHE protons undergo efficient photomeson interactions in dense radiation fields without escaping. This favors small values of R or Γ that are contrary to and almost mutually exclusive with the UHECR criterion, as shown in Asano (2005) (see also Gialis & Pelletier 2005). For example, the requirement that the emitted neutrino fluence $> 10^{-5}$ erg cm $^{-2}$ in the current model corresponds well with $\Gamma \lesssim 300(\Delta t/0.1\text{s})^{-0.3}(E_{\text{sh}}/10^{51}\text{erg})^{0.2}$, entirely the opposite of the UHECR bound above. (See §C for a summary of the neutrino spectra in the current model.) Taking this constraint at face value, we can find some overlap with the lowest Γ cases with GeV-TeV components in Figs. 7 and 8. Indeed, the pertinent process is found to be secondary pair synchrotron emission, which is generated together with neutrinos in $p\gamma$ interactions. Yet there is also a large parameter space with even lower Γ that allows copious neutrino emission but very little gamma-ray or UHECR production. Although neutrino observations will still be indispensable to verify that UHE proton acceleration actually occurs in GRBs, the bursts that emit the most neutrinos may not be the ones that contribute the most UHECRs. (Such remarks do not apply if UHECR acceleration can occur in external shocks; Vietri 1995; Waxman & Bahcall 2000; Dermer 2002) (see however Gallant & Achterberg 1999; Milosavljević & Nakar 2006, regarding external forward shocks.)

Thus we find that the connection between UHECR, neutrino, and gamma-ray production in GRB internal shocks is very intimate, but not one-to-one and nontrivial (see also Dermer et al. 2007). Further studies are warranted for a more complete understanding, but this point should be important to bear in mind for the respective observations.

We remark that all of the above discussion is based on the assumption $U_p = U_e$ (§2.1). However, recent, post-SWIFT observations reveal the GRB redshift distribution to be skewed to higher z than previously believed (Jakobsson et al. 2006). This may suggest that a larger energy budget with $U_p > U_e$ may be necessary for GRB UHECR scenarios to remain viable, implying correspondingly higher gamma-ray and neutrino contributions. (Note that extreme values such as $U_p \sim 10^3 U_e$

have also been proposed; Totani 1998).

6. OBSERVATIONAL IMPLICATIONS

Here we briefly comment on the implications for existing and future observations.

Some EGRET-detected GRBs exhibited GeV emission coinciding with the prompt emission, with spectra that are mostly consistent with an extrapolation of the MeV spectra (Dingus 2001). For GRB 940217, there is some evidence of a separate high-energy component during the prompt phase, and perhaps in the delayed, hour-timescale emission as well (Hurley et al. 1994) (see also Dermer 2005). While the latter is likely to be associated with the external shock (e.g. Mészáros & Rees 1994; Böttcher & Dermer 1998; Zhang & Mészáros 2001; Inoue et al. 2003), the former could possibly be related to some of the emission processes discussed here. More information is necessary to be conclusive, however. A markedly distinct component with a hard spectrum above several MeV was seen in GRB 941017 (González et al. 2003), but the fact that it varied on considerably longer timescales compared to the sub-MeV emission may favor an external shock origin (e.g. Granot & Guetta 2003; Pe'er & Waxman 2004a; Dermer & Atoyan 2004; Beloborodov 2005). At any rate, much more detailed studies of the GeV prompt emission should become feasible soon after the launch of GLAST, which may detect some or all of the emission components discussed here.

Although clear detections have yet to be achieved at TeV energies, the MAGIC telescope has conducted rapid follow-up observations for selected GRBs, in some cases overlapping with the prompt emission phase (Albert et al. 2006, 2007). The obtained upper limits reach fluence levels of $< 10^{-7}$ erg cm $^{-2}$ at ~ 0.1 TeV with integration times of several minutes, so our fiducial $z = 0.1$ burst should be readily detectable. Estimating the amount of intergalactic attenuation with the baseline background model of Kneiske et al. (2004), MAGIC may be able to detect the proton synchrotron emission of Fig. 3 or muon synchrotron emission of Fig. 6 out to $z \lesssim 1$, and the IC emission of Fig. 2 to somewhat higher z , approaching the typical redshifts of GRBs. Thus the prospects are very promising for further observations by MAGIC as well as other Cerenkov telescopes such as H.E.S.S., VERITAS and CANGAROO III, and especially the near-future upgraded facilities MAGIC II and H.E.S.S. II with their lower energy thresholds.

Weak evidence of TeV photons coincident with GRBs have also been reported by some surface detectors, e.g. MILAGRITO (Atkins et al. 2000). However, the inferred energy fluxes are much higher than at MeV, which is difficult to explain in the current model framework unless extreme parameters are invoked, e.g. $U_p \gg U_e$ (Totani 1998). More observations are anticipated for such facilities with their wide-field monitoring capabilities, including air shower arrays like ARGO-YBJ (Di Girolamo et al. 2004) and even the Pierre Auger Observatory (Allard et al. 2005).

7. CONCLUSIONS AND OUTLOOK

Following the internal shock scenario and focusing on GeV-TeV energies, we have modelled the broadband spectra of GRB prompt emission through detailed Monte

Carlo simulations including a wide variety of physical processes related to high-energy electrons and protons. Besides electron inverse Compton emission, it was shown that interesting proton-induced components such as proton synchrotron, muon synchrotron and secondary pair synchrotron emission can become clearly visible. Multiple component spectra with double breaks may offer unique evidence of ultra-high-energy proton acceleration. The conditions favorable for GeV-TeV emission may also imply efficient UHECR acceleration and escape, but not necessarily strong neutrino emission.

The observational prospects are very promising for GLAST, Cerenkov telescopes such as MAGIC (II), H.E.S.S. (II), VERITAS and CANGAROO III, as well as wide-field surface detector facilities. Such observations should test the internal shock model of the prompt emission, provide new insights into the physics of GRB outflows and central engines, and probe the origin of UHECRs.

Note that since we did not explicitly treat the dynamics of internal shock formation, some aspects of our study may also be valid in more general scenarios, e.g. models involving magnetic energy dissipation (e.g. Fox & Mészáros 2006, and references therein), if electrons and protons can be accelerated with similar energy distributions.

Our Monte Carlo simulations have also allowed detailed studies of the prompt optical emission, with interesting new results concerning both electron- and proton-

induced spectral components. This will be the subject of a separate paper (Asano & Inoue, in preparation).

More detailed and comprehensive investigations of the current problem should accommodate a wider range of parameters, including dispersions in ε_{pk} , β and E_{tot} , as well as the variety of pulse properties (e.g. Zhang & Mészáros 2002; Asano & Kobayashi 2003). Accounting for time variability is also an important goal for the future. We note that such effects may potentially smooth out some of the more subtler spectral features discussed here and hinder their observational discrimination, except for the case of sufficiently bright brights where time-resolved spectra can be acquired. Our detailed formalism for calculating complicated hadronic interactions and pair cascades should also be useful for other applications, such as high-energy emission from the afterglow phase (Böttcher & Dermer 1998; Derishev et al. 1999; Sari & Esin 2001; Zhang & Mészáros 2001; Pe'er & Waxman 2005).

As this work was being completed, we became aware of a preprint by Gupta & Zhang (2007) that addresses issues similar to this paper, albeit it with a simpler, analytic formulation.

We thank F. Aharonian, Z. Bosnjak, E. Parizot, M. Teshima and especially F. Daigne for very valuable discussions.

APPENDIX

INVERSE COMPTON SPECTRA

When IC emission is dominant at high-energies (§3.2), the IC peak energy ε_{IC} and the IC to synchrotron peak fluence ($\varepsilon f(\varepsilon)$) ratio may allow a useful consistency check of the internal shock model within the parameter space of the present study (§2.2). In Fig. 9, we summarize the dependence of these two quantities on Δt , E_{sh} , Γ and f_B . Roughly speaking, $\varepsilon_{\text{IC}} \propto \Gamma^{4.5} E_{\text{sh}}^{-1} \Delta t^{1.5}$, which is similar to the expression for ε_{cut} (§3.1) and sensitive to Γ . The peak fluence ratio does not vary monotonically with E_{sh} as it is affected by $\gamma\gamma$ absorption at large E_{sh} . The IC peak is suppressed for larger f_B and disappears for $f_B = 30$.

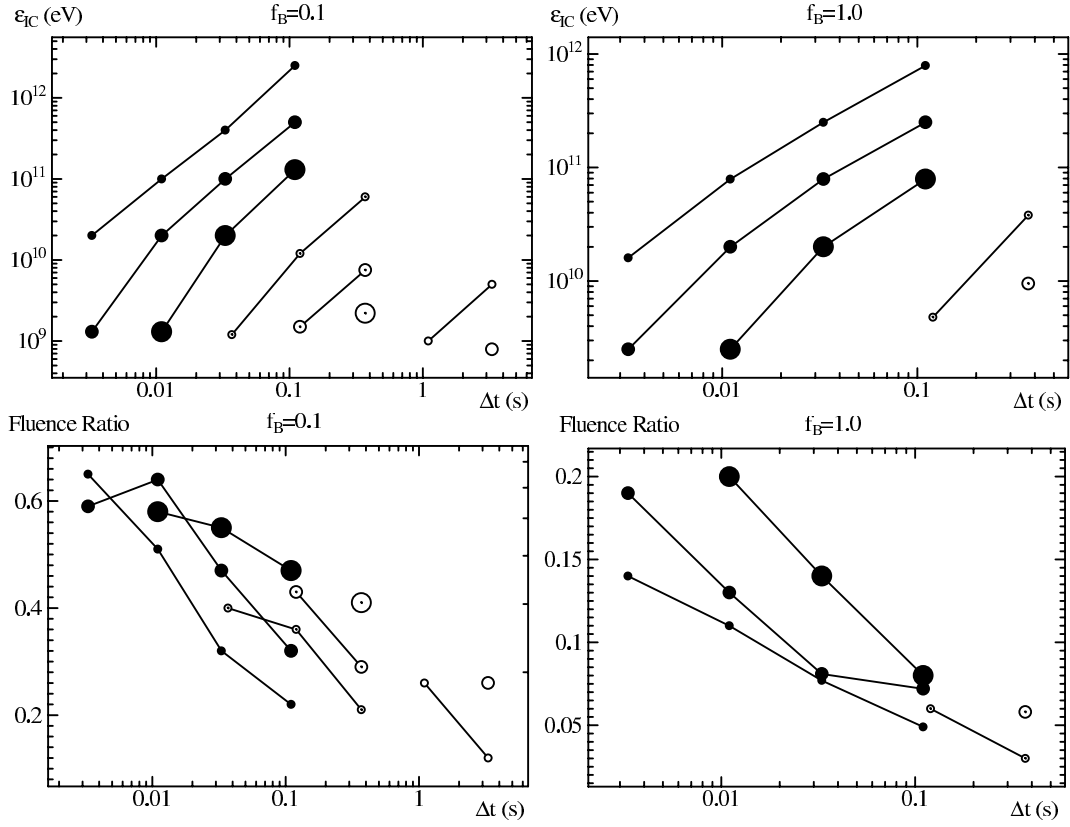


FIG. 9.— IC peak energy ε_{IC} (upper panels) and IC to synchrotron peak fluence ratio (lower panels), for $f_B = 0.1$ (left) and $f_B = 1.0$ (right). Open, dotted and filled circles represent $\Gamma = 100, 300$ and 1000 , while small, medium and large circle size correspond to $E_{sh} = 10^{50}, 10^{51}$ and 10^{52} erg, respectively.

SUMMARY OF HIGH-ENERGY SPECTRA

A large variety of high-energy spectra are realized in the current model. Those with a clear excess above a simple extrapolation of the MeV-band spectrum are summarized quantitatively in the Δt - E_{sh} parameter plane in Fig. 10.

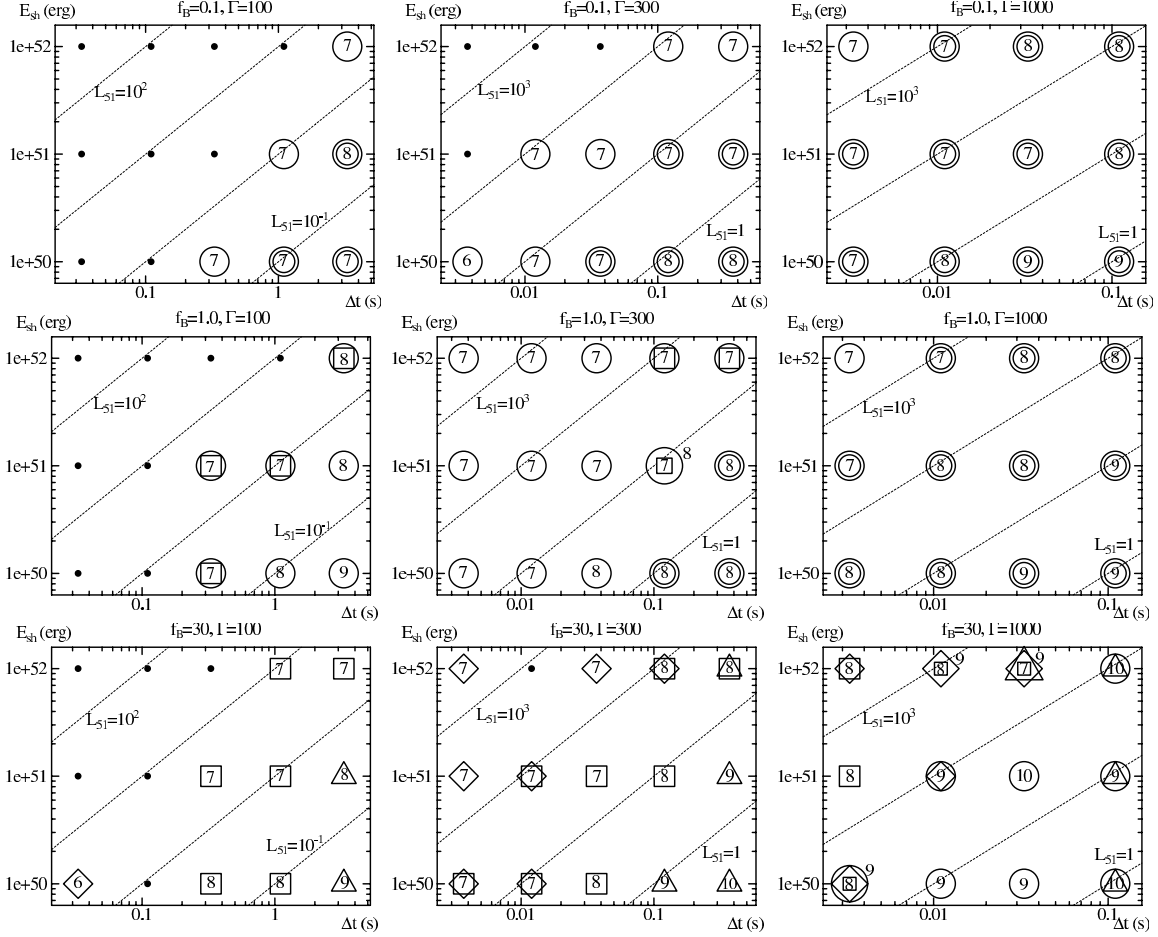


FIG. 10.— Summary of high-energy spectral components in the Δt - E_{sh} plane, with f_B and Γ denoted above each panel. Dotted lines indicate equal luminosity at unit logarithmic intervals normalized by $L_{51} = L/10^{51} \text{ erg s}^{-1}$. The symbols designate the relevant emission process; circles, rectangles, diamonds and triangles respectively signify IC, secondary pair synchrotron, muon synchrotron and proton synchrotron emission. Double circles are cases of IC emission with distinct second peaks. The number inside the symbol is the photon energy where the emission component becomes apparent in log eV units. Two overlapping symbols imply that the respective components occur at similar photon energies, whereas one symbol encircled by another stand for double breaks, with the corresponding break energies in log eV inscribed beside each symbol.

NEUTRINO SPECTRA

In the current model, two types of neutrino spectra can occur (Asano 2005; Asano & Nagataki 2006). When photopion cooling of protons is efficient, the neutrino number spectrum $\propto \varepsilon_\nu^{-2}$ reflecting that of protons, with a high-energy break at which the synchrotron cooling time of the parent pion or muon equals their lifetime (Rachen & Mészáros 1998), and a low energy break at which the photopion cooling time of the parent proton equals t_{exp} . In contrast, for inefficient photopion cooling, the spectrum has only one break corresponding to the latter and no portion $\propto \varepsilon_\nu^{-2}$. Fig. 11 summarizes these characteristic break energies $\varepsilon_{\nu b}$ when the neutrino fluence $> 10^{-5} \text{ erg cm}^{-2}$. An analytical estimate for the high-energy break gives $\varepsilon_{\nu b} \propto \Gamma B^{-1} \propto \Gamma R^{1.5} E_{\text{sh}}^{-0.5} \propto \Gamma^4 \Delta t^{1.5} E_{\text{sh}}^{-0.5}$, which agrees with our numerical results.

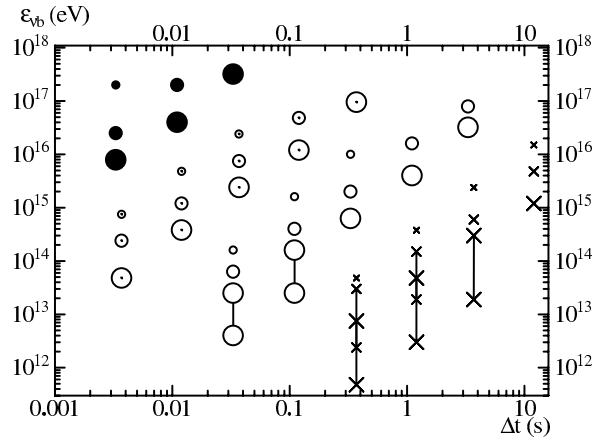


FIG. 11.— Neutrino break energy $\varepsilon_{\nu b}$ versus Δt , for $f_B = 1.0$. Crosses, open, dotted and filled circles represent $\Gamma = 30, 100, 300$ and 1000 , while small, medium and large symbol size correspond to $E_{sh} = 10^{50}, 10^{51}$ and 10^{52} erg, respectively. For cases with two breaks, they are joined by a vertical line.

REFERENCES

Aharonian, F. et al. 2006, *Nature*, 446, 1018
 Albert, J. et al. 2006, *ApJ*, 641, L9
 Albert, J. et al. *ApJ*, submitted (astro-ph/0612548)
 Allard, D. et al. 29th ICRC, 4, 427
 Amati, L. 2006, *MNRAS*, 372, 233
 Asano, K. 2005, *ApJ*, 623, 967
 Asano, K., & Iwamoto, S. 2002, *ApJ*, 581, 381
 Asano, K., & Kobayashi, S. 2003, *PASJ*, 55, 579
 Asano, K., & Nagataki, S. 2006, *ApJ*, 640, L9
 Asano, K., & Takahara, F. 2003, *PASJ*, 55, 433
 Atkins, R. et al. 2000, *ApJ*, 533, L119
 Atkins, R. et al. 2005, *ApJ*, 630, 996
 Baring, M. G. 2006, *ApJ*, 650, 1004
 Baring, M. G., & Harding, A. K. 1997, *ApJ*, 491, 663
 Baring, M. G., & Kirk, J. G. 1991, *A&A*, 241, 329
 Beloborodov, A. M. 2005, *ApJ*, 618, L13
 Berestetskii, V. B., Lifshitz, E. M., & Pitaevskii, L. P. 1982, *Quantum Electrodynamics* (New York: Pergamon), p. 371
 Böttcher, M., & Dermer, C. D. 1998, *ApJ*, 499, L134
 Blumenthal, G. R., & Gould, R. J. 1970, *Rev. Mod. Phys.*, 42, 237
 Casanova, S., Dingus, B. L., & Zhang, B. 2007, *ApJ*, 656, 306
 Connaughton, V. et al. 1997, *ApJ*, 479, 859
 Daigne, F., & Mochkovich 1998, *MNRAS*, 296, 275
 Derishev, E. V., Kocharovsky, V. V., & Kocharovsky, V. V. 1999, *ApJ*, 521, 640
 Dermer, C. D. 2002, *ApJ*, 574, 65
 Dermer, C. D. astro-ph/0512164
 Dermer, C. D., & Atoyan, A. 2004, *A&A*, 418, L5
 Dermer, C. D., & Atoyan, A. 2006, *New J. of Phys.* 8, 122
 Dermer, C. D., Ramirez-Ruiz, E., & Le, T. 2007, *ApJ*, 664, L67
 Di Girolamo, T., Di Sciacio, G., & Vernetto, S. 2004, astro-ph/0401272
 Dingus, B. 2001, in *High Energy Gamma Ray Astronomy*, ed. F. A. Aharonian and H. J. Völk, AIP 558, 383
 Erber, T. 1966, *Rev. Mod. Phys.*, 38, 626
 Fox, D. B., & Mészáros, P. 2006, *New J. of Phys.* 8, 199
 Gallant, Y. A., & Achterberg, A. 1999, *MNRAS*, 305, L6
 Ghisellini, G., & Svensson, R. 1991, *MNRAS*, 252, 313
 Gialis, D., & Pelletier, G. 2005, *ApJ*, 627, 868
 González, M. M., et al. 2003, *Nature*, 424, 749
 Granot, J., & Guetta, D. 2003, *ApJ*, 598, L11
 Guetta, D., & Granot, J. 2003, *ApJ*, 585, 885
 Gupta, N., & Zhang, B., *MNRAS*, submitted (arXiv:0704.1329)
 Halzen, F., & Hooper, D. 2002, *Rep. Prog. Phys.*, 65, 1025
 Horan, D. et al. 2007, *ApJ*, submitted (astro-ph/0701281)
 Hurley, K. et al., 1994, *Nature*, 372, 652
 Inoue, S. 2007, in *Energy Budget in the High Energy Universe*, Eds. K. Sato and J. Hisano, World Scientific (astro-ph/0701835)
 Inoue, S., Guetta, D., & Pacini, F. 2003, *ApJ*, 583, 379
 Jakobsson, P. et al., *A&A*, 447, 897
 Kneiske, T. M., Bretz, M., Mannheim, K., & Hartmann, D. H. 2004, *A&A*, 413, 807
 Kobayashi, S., Piran, T., & Sari, R. 1997, *ApJ*, 490, 92
 Lithwick, Y., & Sari, R. 2001, *ApJ*, 555, 540
 Malkov, M. A., & Drury, L. O’C. 2001, *Rep. Prog. Phys.*, 64, 429
 Mannheim, K., Hartmann, D., & Funk, B. 1996, *ApJ*, 467, 532
 Mészáros, P. 2006, *Rep. Prog. Phys.*, 69, 2259
 Mészáros, P., & Razzaque, S. 2006, in *Energy Budget in the High Energy Universe*, Eds. K. Sato and J. Hisano, World Scientific (astro-ph/0605166)
 Mészáros, P., & Rees, M. J. 1994, *MNRAS*, 269, L41
 Mészáros, P., & Rees, M. J. 2000, *ApJ*, 530, 292
 Milosavljević, M., & Nakar, E. 2006, *ApJ*, 651, 979
 Murase, K., Asano, K., & Nagataki, S. 2007, *ApJ*, submitted (astro-ph/0703759)
 Papatthanassiou, H., & Mészáros, P. 1996, *ApJ*, 471, L91
 Pe’er, A., & Waxman, E. 2004a, *ApJ*, 603, L4
 Pe’er, A., & Waxman, E. 2004b, *ApJ*, 613, 448
 Pe’er, A., & Waxman, E. 2005, *ApJ*, 633, 1018
 Pilla, R. P., & Loeb, A. 1998, *ApJ*, 494, L167
 Piran, T. 2005, *Rev. Mod. Phys.*, 76, 1143
 Plaga, R. 1995, *Nature*, 374, 430
 Preece, R. D., Briggs, M. S., Mallozzi, R. S., Pendleton, G. N., Paciesas, W. S., & Band, D. L. 2000, *ApJS*, 126, 19
 Rachen, J. P., & Mészáros, P. 1998, *Phys. Rev. D*, 58, 123005
 Razzaque, S., Mészáros, P., & Zhang, B. 2004, *ApJ*, 613, 1072
 Rees, M. J., & Mészáros, P. 1994, *ApJ*, 430, L93
 Sari, R., & Esin, A. A., *ApJ*, 548, 787
 Sari, R., & Piran, T. 1997, *ApJ*, 485, 270
 Schadmand, S. 2003, *Eur. Phys. J. A*, 18, 405
 Totani, T. 1998, *ApJ*, 509, L81
 Torres, D., & Anchordoqui, L. A. 2004, *Rep. Prog. Phys.*, 67, 1663
 Vietri, M. 1995, *ApJ*, 453, 883
 Vietri, M. 1997, *Phys. Rev. Lett.*, 78, 4328
 Wang, X. Y., Cheng, K. S., Dai, Z. G., & Lu, T. 2004, *ApJ*, 604, 306
 Waxman, E. 1995, *Phys. Rev. Lett.*, 75, 386
 Waxman, E., & Bahcall, J. N. 1997, *Phys. Rev. Lett.*, 78, 2292
 Waxman, E., & Bahcall, J. N. 2000, *ApJ*, 541, 707
 Zhang, B., & Kobayashi, S. 2005, *ApJ*, 628, 315
 Zhang, B., & Mészáros, P. 2001, *ApJ*, 559, 110
 Zhang, B., & Mészáros, P. 2002, *ApJ*, 581, 1236
 Zhang, B., & Mészáros, P. 2004, *IJMPA*, 19, 2385
 Zhang, B. et al. 2007, *ApJ*, 655, 989